GAS-PARTICLE FLOW IN A DIFFUSER

Francisco José de Souza
Ana Luiza Silva
Jonathan Utzig
Faculdade de Engenharia Mecânica
Universidade Federal de Uberlândia
e-mails: fjsouza@mecanica.ufu.br,

Abstract. In this work, a numerical investigation on the gas-particle flow in a vertical diffuser is carried out. This study was motivated by the experimental work of by Kale and Eaton (1984), who noticed that the fully attached flow in a diffuser in the freeboard region of a particle bed would become detached if no particles were present. It was concluded at the time that this effect was not caused by the high inlet turbulence levels, but rather by the particles. With the goal to better understand the interactions between the particles and the fluid in a diffuser, simulations of the particle-laden gas flow in a vertical conical diffuser are run using the Euler/Lagrange approach. The model, which includes particle-to-particle collisions, the particle influence on the gas phase and wall roughness effects, is first validated based on experimental results from a horizontal channel and a vertical diffuser for both the continuous and dispersed phases at different mass loadings. Investigations on the effects of particles at different mass loadings and wall roughness on the diffuser flow are then carried out. It has been found that, even at moderate mass loadings, particles can significantly affect the diffuser flow pattern, and actually reattach the otherwise separated flow under some conditions. It has also been found that wall roughness plays a very important role in homogenizing the particle distribution at the diffuser section. The resulting more uniform concentration and velocity profiles can then reenergize the separated boundary layer and reattach it to the wall.

Keywords: four-way coupled simulation, diffuser, gas-solid flow

1. INTRODUCTION

Gas-particle flows are very commonly found in pharmaceutical, chemical and petroleum industries. The optimization of the operations involved normally requires a detailed knowledge of the very intrinsic phenomena that take place within the equipment handling the mixture. Over the past few years, CFD has become an indispensible tool to understand and improve such operations. Although limited to low volumetric fractions, the Euler-Lagrange approach has been intensively used as it provides detailed information on the particle behavior on a microscopic level.

Several theoretical and experimental studies have shown that the presence of particles in fluids affects some characteristics of the turbulence structure (Laín and Sommerfeld, 2012, Breuer and Alletto, 2012). Mostly, it has been found that the addition of small particles tends to attenuate or modulate turbulence and flatten the mean fluid velocity profile, but also increase the pressure drop across channels and pipes, for instance. This results mainly from the particle-to-wall and particle-to-particle collisions, as extensively demonstrated by Laín *et al.* (2002), Laín and Sommerfeld (2012) and Benson *et al.* (2005), to name just a few.

Most of the works above focused on channel or pipe flow, and there are few references on effects of particles on detached flow. In one of them (Fessler and Eaton, 1999), the particle-laden flow in a backward-facing-step, which is well known for its massive separated flow, was investigated experimentally. The detached flow region was found not to be affected by the particles, probably because the large particle inertia avoided their entrapment in the recirculation region. In another (Laín and Sommerfeld, 2013), the particles were seen to give origin to two counter-rotating vortices in bend flow, with effects on the secondary flow, but the detached region was not shown in detail. Breuer and Alletto (2012) used LES to simulate the particle-laden in a model combustion chamber without swirl. They found that, for mass loading 1.1 of glass spheres of 50 micrometers, the recirculation region in the vicinity of the chamber axis was elongated and slightly shifted from the axis. Also, large particles at medium mass loading or small particles at high mass loading sufficed to induce momentum to suppress the stagnation points on the chamber axis.

As in the work of Laín and Sommerfeld (2013) and Breuer and Alletto (2012), particles are known to significantly affect also reverse flow regions. While working with a fluidized bed, Kale and Eaton (1984) incorporated diffusers with different opening angles at the freeboard region to reduce particle elutriation. Contrary to the expected behavior, which was based on the single-phase flow only, the elutriation rate was actually observed to decrease monotonically with the diffuser opening angle. Later (Kale and Eaton, 1985), the gas velocity profiles in the diffuser were measured by means of LDA and the flow, which would be otherwise detached, was found to be attached in the presence of the particle bed. Clearly, because of the particle bed upstream of the diffuser, the gas velocity profile is flatter and turbulence levels are increased, which would help reattach the flow. However, this would not be enough to avoid the backflow in a 60°-angle diffuser, for instance. Therefore, one concludes that the particles are actually responsible for reattaching the flow. Since then, there have been very few investigations on the effects of particles in diffusers. Bohnet and Triesch (2003) studied

the influence of particles on the turbulence in a vertical, conical diffuser. They found that small particles ($Re_p=60$) damped the turbulence, but with increasing particle Reynolds the vortex shedding due to the particles reduced attenuation and actually cause turbulence enhancement. However, no flow detachment or reattachment was reported.

The goal of this study is to better understand the effects of particles on the flow in a diffuser. The focus is on the mechanism for explaining the mitigation/elimination of the backflow when particles are present. With that purpose in mind, the solid-gas flow in the configuration investigated by Bohnet and Triesch (2003) is simulated. The interaction of glass spheres 150 micrometers in diameter and at different mass loadings with the gas is then calculated in diffusers with different wall asperities. It is shown that, depending on the particle diameter and diffuser surface characteristics, mass loadings as low as 0.5 can substantially affect the flow in the diffuser, effectively causing the boundary layer to reattach to the wall.

2. MATHEMATICAL MODELS

As mentioned previously, the Euler-Lagrange approach is employed in this investigation. Below the modeling of both phases is described, accordingly.

2.1 Gas phase model

The numerical solution of the conservation equations for the momentum and turbulence is accomplished by the computational code UNSCYFL3D. This in-house tool is based on the finite volume method in unstructured three-dimensional grids. The SIMPLE (Semi-Implicit Method for Pressure-Linked Equations) algorithm is used to couple the velocity and pressure fields. The collocated arrangement is used for all variables, with the conventional Rhie-Chow interpolation scheme for the computation of the mass flow rate through each volume face. The discretization procedure described above generates a linear system of equations for the conserved variables at the element centers. The biconjugate gradient and the algebraic multigrid (AMG) methods are used to efficiently solve the linear system resulting from the discretization of each conserved variable. The main advantage of this modeling is that it does depend on the element shape, as the data structure is based on element faces. For each element face, arrays containing the number of L and R elements sharing it are created. As it be shown subsequently, all operations involved in transferring information from the Eulerian to the Lagrangian frames and vice-versa utilize either face or element center data, and are therefore also irrespective of the number of faces each element contains. For storing the coefficients of the linear systems for the velocity components, pressure correction and turbulence variables, the CSR (Compressed Sparse Row) format is used. For further information on the method, references Mathur and Murthy (1997) and Ferziger and Peric (2002) are recommended.

In all the simulations carried out in this work only the steady-state solution for fluid was sought. The second-order upwind scheme was employed for the advective term, whereas the centered differencing scheme was used for the diffusive terms of the momentum equations and turbulence model equations.

The standard k-epsilon model is the most widely known and extensively used two-equation eddy viscosity model (Bardina *et al.*, 1997). It was originally developed to improve the mixing-length model and to avoid the algebraic prescription of the turbulence length scale in complex flows. Transport equations are solved for two scalar properties of turbulence, the turbulence kinetic energy, k, and the dissipation rate of turbulent kinetic energy, epsilon:

$$\frac{\partial(\rho u_j k)}{\partial x_j} = \frac{\partial}{\partial x_j}\left[\left(\mu + \frac{\mu_t}{\sigma_k}\right)\frac{\partial k}{\partial x_j}\right] + P - \rho\varepsilon \tag{1}$$

$$\frac{\partial(\rho u_j \varepsilon)}{\partial x_j} = \frac{\partial}{\partial x_j}\left[\left(\mu + \frac{\mu_t}{\sigma_\varepsilon}\right)\frac{\partial \varepsilon}{\partial x_j}\right] + C_{\varepsilon 1}\frac{k}{\varepsilon}P - C_{\varepsilon 2}\rho\frac{\varepsilon^2}{k} \tag{2}$$

where P is the production term, given by:

$$P = (\mu_t + \mu)\left[\left(\frac{\partial u_i}{\partial u_j} + \frac{\partial u_j}{\partial u_i}\right)\frac{\partial u_i}{\partial u_j}\right] \tag{3}$$

The eddy-viscosity in the standard k-epsilon model is defined as a function of the turbulent kinetic energy and the turbulent dissipation rate as:

$$\mu_{t,standard} = C_\mu \rho \frac{k^2}{\varepsilon} \tag{4}$$

Although widely used, the standard k-epsilon displays some weaknesses, such as the assumption that the flow is fully turbulent. To circumvent this issue, the 2-layer k-epsilon model was employed, as it can handle well both the core flow and the near wall region. Essentially, it consists in solving the standard model for the turbulent flow region and a one-equation model for the region affected by the viscosity. In the one-equation k-epsilon model, the conservation equation for *k* is retained, whereas epsilon is computed from:

$$\varepsilon = \frac{k^{3/2}}{l_\varepsilon}$$

(5)

The length scale that appears in Eq. (5) is computed from:

$$l_\varepsilon = y C_l \left(1 - e^{-Re_y/A_\varepsilon}\right)$$

(6)

In Eq. (6), Re_y is the turbulent Reynolds number, defined as:

$$Re_y = \frac{\rho y \sqrt{k}}{\mu}$$

(7)

where *y* is the distance from the wall to the element centers. This number is the demarcation of the two regions, fully turbulent if $Re_y > Re_y^*$, $Re_y^*=200$ and viscosity-affected, $Re_y < 200$. For the one-equation model, the turbulent viscosity is computed from:

$$\mu_{t,2layer} = \rho C_\mu l_\mu \sqrt{k}$$

(8)

The length scale in the equation above is computed as below:

$$l_\mu = y C_l \left(1 - e^{-Re_y/A_\mu}\right)$$

(9)

In UNSCYFL3D, both the standard k-epsilon and the one-equation model described above are solved over the whole domain, and the solutions for the turbulent viscosity and the turbulence kinetic energy dissipation rate provided by both models are smoothly blended:

$$\mu_t = \lambda_\varepsilon \mu_{t,standard} + (1 - \lambda_\varepsilon)\mu_{t,2layer}$$

(10)

A blending function, λ_ε, is defined in such a way that it is equal to unity far from walls and is zero very near walls. The blending function used here is:

$$\lambda_\varepsilon = \frac{1}{2}\left[1 + \tanh\left(\frac{Re_y - Re_y^*}{A}\right)\right]$$

(11)

The constant *A* determines the width of the blending function:

$$A = \frac{0.20 Re_y^*}{\tanh(0.98)}$$

(12)

The purpose of the blending function λ_ε is to prevent solution divergence when the solution from both the standard and the one-equation models do not match. The constants in the length scale formulas, Eqs. (6) and (9), are taken from:

$$c_l = 0.4187 c_\mu^{-3/4} \qquad A_\mu = 70 \qquad A_\varepsilon = 2c_l$$

(13)

Since no wall-functions are used, it is very important to refine the grid so as to have *y+<1* in the first element away from the wall and ensure accurate results for the fluid flow.

Finally, the carrier fluid "feels" the presence of particles as an additional source term in the momentum equation. This term is modeled based on Newton's second and third laws:

$$S_{p,Ui} = -n \left\langle m_p \left(\frac{du_{pi}}{dt} - \left(1 - \frac{\rho}{\rho_p}\right) g_i\right)\right\rangle$$

(14)

n is the average number of real particles per unit volume in the control volume, m_p is the particle mass, u_{pi} is the particle velocity, ρ_p is the particle material density, ρ is the fluid density and g_i is the gravity vector. The brackets denote mean values over all particle realizations in that particular control volume. Thus, for each computational particle crossing a control volume, one contribution is added to the source-term above.

2.2 Particle motion model

As mentioned in the previous section, the dispersed phase is treated in a Lagrangian framework, in which each particle is tracked through the domain and its equation of motion is based on Newton's second law. The trajectory, linear momentum and angular momentum conservation equations for a rigid, spherical particle can be written, respectively, as:

$$\frac{dx_{pi}}{dt} = u_{pi} \tag{15}$$

$$m_p \frac{du_{pi}}{dt} = m_p \frac{3\rho C_D}{4\rho_p d_p}(u_i - u_{pi}) + F_{si} + F_{ri} + \left(1 - \frac{\rho}{\rho_p}\right)m_p g_i \tag{16}$$

$$I_p \frac{d\omega_{pi}}{dt} = T_i \tag{17}$$

In the above equations, $u_i = U_i + u_i$ are the components of the instantaneous fluid velocity. The average fluid velocity U_i is interpolated from the resolved flow field, whereas the fluctuating component u_i is calculated according to the Langevin dispersion model. d_p is the particle diameter and $I_p = 0.1 m_p d_p^2$ is the moment of inertia for a sphere.

The empirical correlation proposed by Schiller and Naumann (1935) is used to evaluate the drag coefficient past each particle:

$$C_D = 24 Re_p^{-1}\left(1 + 0.15 Re_p^{0.687}\right) \quad if \; Re_p < 1000$$
$$C_D = 0.44 \quad if \; Re_p > 1000 \tag{18}$$

In Eq. (18), Re_p is the particle Reynolds number $Re_p = \rho d_p |\vec{u} - \vec{u}_p|/\mu$.

The calculation of the shear-induced lift force is based on the analytical result of Saffman (1965) and extended for higher particle Reynolds numbers according to Mei (1992):

$$\vec{F}_s = 1.615 d_p \mu Re_s^{1/2} C_{ls}\left[(\vec{u} - \vec{u}_p) \; x \; \vec{\omega}\right] \tag{19}$$

$\vec{\omega}$ is the vorticity, $Re_s = \rho d_p^2 |\vec{\omega}|/\mu$ is the particle Reynolds number of the shear flow and $C_{ls} = F_{ls}/F_{ls,Saff}$ represents the ratio of the extend lift force to the Saffman force:

$$C_{ls} = (1 - 0.3314\beta^{0.5})e^{-0.1 Re_p} + 0.3314\beta^{0.5} \quad if \; Re_p < 40$$
$$C_{ls} = 0.0524\left(\beta Re_p\right)^{0.5} \quad if \; Re_p > 40 \tag{20}$$

β is a parameter $\beta = 0.5 Re_s / Re_p (0.005 < \beta < 0.4)$.

The rotation-induced lift is computed based on the relation given by Rubinow and Keller (1961), which was extended to account for the relative motion between particle and fluid:

$$\vec{F}_r = \frac{\pi}{8}\rho d_p^3 \frac{Re_p}{Re_r} C_{lr} \frac{\left[\vec{\Omega} \; x \; (\vec{u} - \vec{u}_p)\right]}{|\vec{\Omega}|} \tag{21}$$

In Eq. (21), $\vec{\Omega} = 0.5\vec{\nabla} \times \vec{u} - \vec{\omega}_p$ and $Re_s = \rho d_p^2 |\vec{\Omega}|/\mu$. The lift coefficient C_{lr} is obtained from the correlation proposed by Lun and Liu (1997):

$$C_{lr} = \frac{Re_r}{Re_p} \quad if \; Re_p < 1$$
$$C_{lr} = \frac{Re_r}{Re_p}\left(0.178 + 0.822 Re_p^{-0.522}\right) \quad if \; Re_p > 1 \tag{22}$$

Also, the rotating particle experiences torque from the fluid flow. The correlation of Rubinow and Keller (1961) was extended to account for the relative motion between fluid and particle at higher Reynolds number:

$$\vec{T} = C_r \frac{\rho d_p^5}{64} \left| \overrightarrow{} \right| \overrightarrow{}$$ (23)

The coefficient of rotation, C_r, was obtained from the following correlation, derived from and the direct numerical simulations of Dennis *et al.* (1980):

$$C_r = \frac{64\pi}{Re_r} \quad if \ Re_r < 32$$
$$C_r = \frac{12.9}{\sqrt{Re_r}} + \frac{128.4}{Re_r} \quad if \ Re_r > 32$$ (24)

Forces such as Basset and virtual mass have been neglected. This is a reasonable assumption since the particle material density is over 1000 times the gas density (Crowe *et al.*, 1998 and Crowe, 2006).

The extension of the Euler/Lagrange approach to unstructured meshes requires the use of accurate interpolation schemes, since in the above equations the continuous phase properties must be determined at the particle center. A few interpolation schemes have been tried out, and the best compromise between accuracy and cost was obtained with the Sheppard's scheme. Basically, the velocity and vorticity components at the particle position are calculated by weighing the neighboring element values with their inverse distances from their centers to the particle position. For integrating the ordinary differential equations (24), (25) and (26), the analytical scheme was used for the linear and angular velocities.

Upon a particle colliding with a wall, the new particle linear and angular velocities after rebound are calculated according to the following conservation equations (Breuer *et al.*, 2012):

Nonsliding collision:

$$\vec{u}_p^+ = \vec{u}_p^- - \frac{2}{7}\vec{u}_{pr}^- - (1 + e)(\vec{u}_p^-.\vec{n})\vec{n}$$ (25)

$$\vec{\omega}_p^+ = \vec{\omega}_p^- - \frac{10}{7}\frac{\vec{n}}{d_p} \ x \ \vec{u}_{pr}^-$$ (26)

Sliding collision:

$$\vec{u}_p^+ = \vec{u}_p^- - (1 + e)(\vec{u}_p^-.\vec{n})\left[\mu_d \frac{\vec{u}_p^-}{|\vec{u}_p^-|} + \vec{n}\right]$$ (27)

$$\vec{\omega}_p^+ = \vec{\omega}_p^- - \frac{5}{d_p}(1 + e)(\vec{u}_p^-.\vec{n})\frac{\mu_d}{|\vec{u}_p^-|} \ \vec{n} \ x \ \vec{u}_{pr}^-$$ (28)

In the above equations, the superscripts – and + denote values prior to and after the collision, respectively, e is the normal restitution coefficient and μ_d is the dynamic friction coefficient. $\vec{n}$ is the normal unit vector pointing outwards of the element face being impacted. $\vec{u}_{pr}$ is the relative velocity at the contact point:

$$\vec{u}_{pr} = \vec{u}_p - (\vec{u}_p.\vec{n})\vec{n} + \frac{d_p}{2}\omega_p \ x \ \vec{n}$$ (29)

Numerous experimental studies have shown evidence that wall roughness and interparticle-collisions are important even at low solid loadings. Therefore, their influence must be included in the modeling. As demonstrated by Laín *et al.* (2008), the wall roughness plays a vital role in the dispersion of particles in pneumatic transport systems. In order to account for such effects, we implemented the model proposed by Sommerfeld and Huber (1999), to represent the effects of surface asperities on the particle flow. In summary, the wall roughness is simulated by assuming that the effective impact angle α is composed of the geometric impact angle $\alpha_{geometric}$ added to a stochastic contribution due to wall roughness.

$$\alpha = \alpha_{geometric} + \xi.\Delta\gamma$$ (30)

This stochastic contribution is sampled from a Gaussian distribution with a standard deviation $\Delta\gamma$, which depends on the structure of wall roughness and particle size. Unfortunately, the value of $\Delta\gamma$ must be calibrated so as to provide the best agreement between the experimental and simulated pressure losses.

Inter-particle collisions are modeled with a stochastic, hard-sphere model. As described by Oesterlé and Petitjean (1993) and Sommerfeld (2001), for each computational particle, a fictitious collision partner is generated, and the probability of a collision is checked based on an analogy with the kinetic theory of gases. This in turn requires that the average ad RMS linear and angular velocities, as well as the particle concentration in each control volume, be sampled and stored every Lagrangian calculation. Although demanding a lot of memory, the method is rather economical and effective, and avoids the use of a deterministic collision model, which is quite expensive computationally. In both interparticle and particle-to-wall collisions, the restitution and friction coefficients were set to 0.9 and 0.4, respectively.

When a structured grid is used, it is simple to determine the element hosting the particle, as there is a straightforward relationship between the element index and its physical location. Because an unstructured grid is used in this work, there is the need for a specific algorithm to locate the particle after its final position is calculated by the integration of Eq. (24). For that purpose, the particle-localization algorithm proposed by Haselbacher *et al.* (2007) was implemented. This algorithm is based on tracking a particle along its trajectory by computing the intersections of the trajectory and the element faces. Since it does not depend on the element topology, it is suitable for use in unstructured grids. Furthermore, it was observed to be extremely faster than costly, direct-search algorithms.

The coupled solution of the continuous and particle phases is summarized as follows (Laín and Sommerfeld, 2012): first the steady-state solution for the fluid phase without particles is computed. Subsequently, at least 250,000 particles are injected and tracked throughout the domain. For each control volume, the average and rms linear and angular velocities, the particle concentration and the source-terms for the fluid momentum equations are stored. After all the particles have left the domain, the fluid flow is solved again, now considering the source-terms sampled during the previous particle calculation. This process is repeated, taking the particle-to-particle collision into account, until a converged solution for both phases is reached. It is important to bear in mind that the particle statistics must be corrected during each particle calculation. Normally, 50 coupling iterations are sufficient for convergence of both phases, which take a couple of hours on a single Intel i7 processor.

3. RESULTS AND DISCUSSION

3.1 Validation of the models

In order to validate the Euler/Lagrange approach extension to unstructured grids, a set of simulations was carried out to reproduce literature data. Firstly, as can be seen in the previous work of Souza *et al.* (2012), the UNSCYFL3D particle-phase model was validated for cyclone flows. Two cyclone geometries with distinct operating conditions were computed, showing good agreement in gas velocities and grade efficiency analyzes with the experiments. Secondly, the mean and RMS results for the particulate phase in the flow of air loaded with glass spheres a horizontal channel have been chosen. Although the channel is a simple geometry, there is a large body of reliable experimental results (Laín and Sommerfeld, 2012, Laín *et al.*, 2002). In this case, we use an average inlet velocity of 20 m/s, monodispersed particles of diameter 130 micrometers at a mass loading of 1.0. The channel wall roughness parameter $\Delta\gamma$ was set to 1.6° for both upper and lower walls. Figure 1 show the comparison between the simulated and experimental results. All comparisons are made at fully developed flow region. It can be seen from Fig. 1 that the results agree well with the experiments. Since the simulation results depend on the correct implementation of a number of models, it can be concluded that the code is validated.
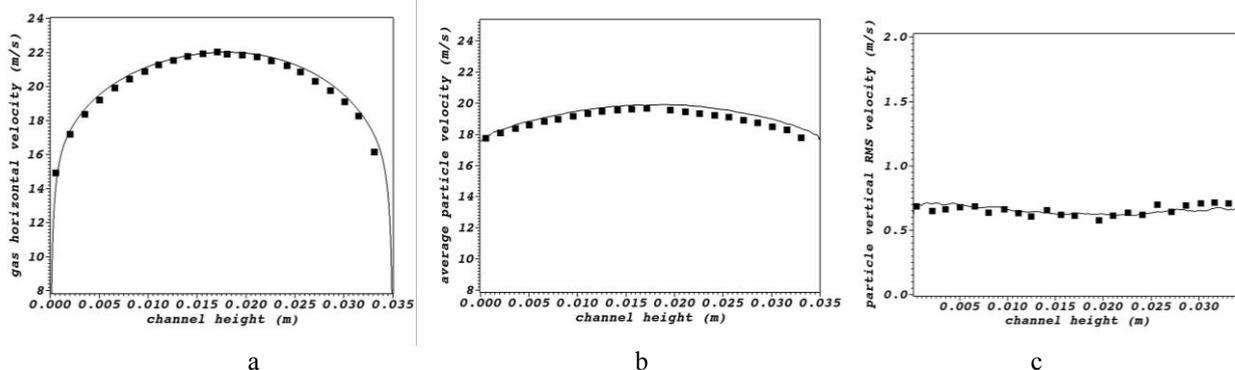
Figure 1. Average gas (a), average particle (b) and RMS particle (c) streamwise velocities for channel flow. Symbols represent experiments by Laín and Sommerfeld (2012) and the line the four-way coupled simulation results.

3.2 Gas-solid flow in a diffuser

As a reference to the parametric investigations to be shown subsequently, the empirical results obtained by Bohnet and Triesch (2003) for a conical diffuser were also used for comparison with the simulations. Part of the mesh containing the diffuser body, used in all the simulations, is shown in Fig. 6. The resolution is nearly 500,000 hexahedra, which provided mesh independent results. The pipe diameters upstream and downstream of the diffuser are 0.029 and 0.0523 m, respectively, and the opening angle is 6°. The flow inlet is placed 5 m upstream of the diffuser in order to ensure that a fully developed flow profile is achieved. The inlet velocity is 25 m/s. The effects of a mass loading 0.5 of monodisperse particles of diameter 150 micrometers are shown in Fig. 7. This simulation will be referred to as smooth wall case, since the parameter describing the wall in the stochastic roughness model, $\Delta\gamma$, was set to 1°.
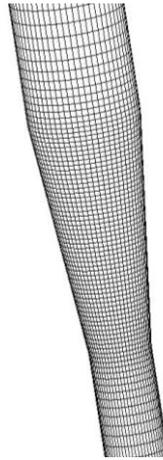
Figure 6. Detail of the mesh used in the diffuser simulations.

a   b
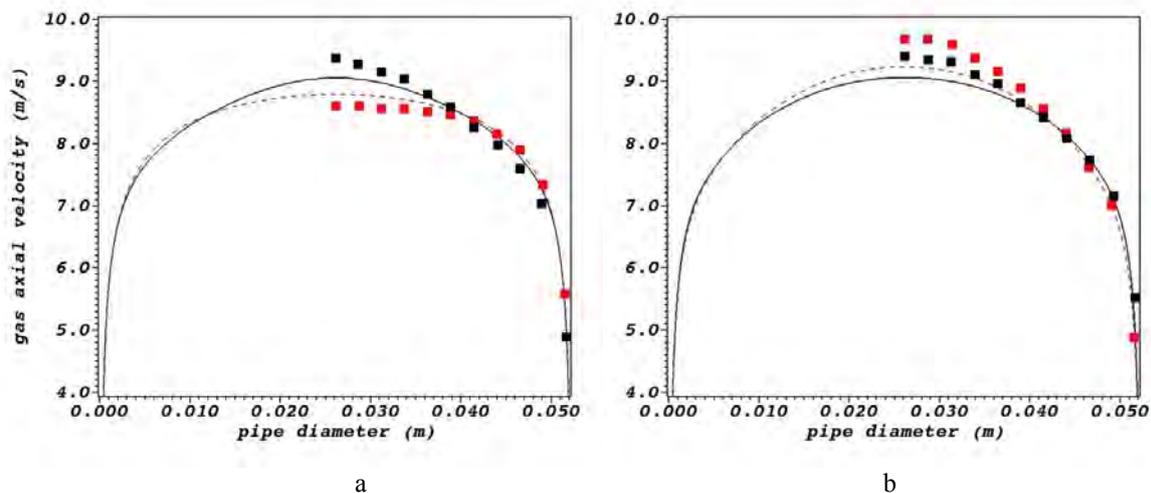
Figure 7. Effect of particles on the average gas axial velocity at 0.7 m (a) and 2.2 m (b) downstream of the diffuser. Red symbols: experimental clean flow, black symbols: experimental gas velocity, dashed line: single-phase flow simulation, full line: four-way simulation of two-phase flow.

Reasonably good agreement is obtained, mainly considering that, because of the turbulence modeling, the average gas velocity is either underpredicted or overpredicted in the core region of the single-phase flow. It should be emphasized at this point that the turbulence produced by the particle wake is not considered in the model, and this is likely to cause some divergence from experiments. Nonetheless, the trends are correctly captured. Noticeably, both experiment and simulation show that at 0.7 m downstream of the diffuser the particle-laden flow is faster in the core region, whereas the opposite effect is observed further downstream (Fig. 7b). This can be explained based on the particle behavior at the diffuser. Figure 8a shows the average particle axial velocity at both positions. It can be seen that closer to the diffuser (at 0.7 m downstream), the particle velocity in the center of the pipe is higher than that of the gas (Fig. 7a), while it reduces to a value lower than the fluid at 2.2 m. As described in section 2.2, different forces act on the particles, but the most relevant are probably the drag, which is proportional to the relative velocity, and gravity.

Souza, F. J., Silva A, L. and Utzig, J.
Gas-particle flow in a diffuser

Because the relative velocity at 0.7 m is negative in the core flow, the particles actually transfer momentum to the gas in this region, and the opposite occurs at 2.2 m aft the diffuser. Conversely, right after the diffuser body, the particles are "pushing" the gas upwards in the core flow, whereas they are retarding the air further downstream. In a straight vertical pipe, typically the relative velocity is positive, as it is at 2.2 m after the diffuser, because gravity and drag tend to slow down the particles.

The next point to be clarified is why the particles flow faster than the fluid downstream of the diffuser. Basically, the gas flow expands inside the diffuser, and consequently, its velocity diminishes. Unlike the fluid, the particles do not expand as much when they enter the diffuser body and their velocity reduction is rather small. Because of their inertia, their axial velocity actually remains very close to that of the inlet pipe. This behavior can be verified in Fig. 8b. Also, it can then be concluded that the particles will experience an overall drag reduction. Further downstream of the diffuser, both the gas and the particle flows will redevelop, and the straight pipe behavior, as shown in Fig. 7b, will be recovered.
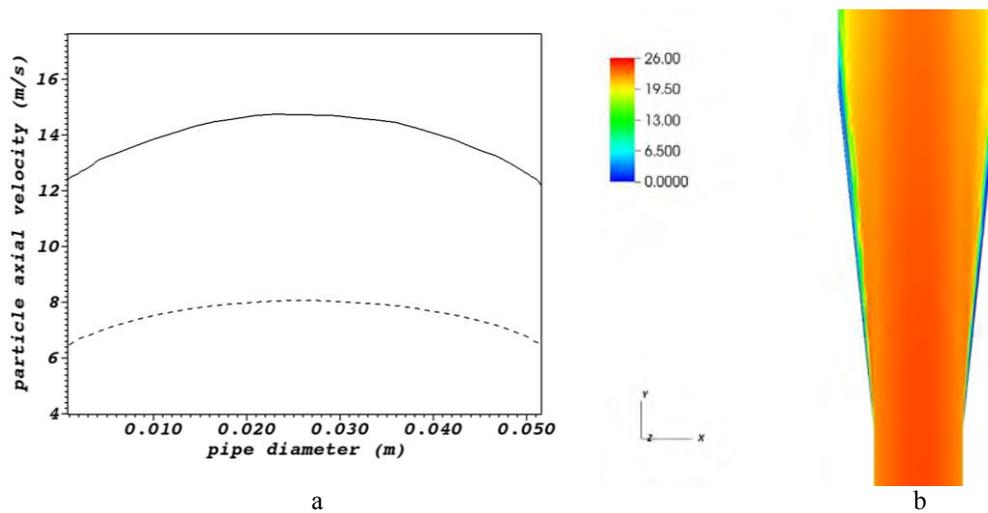
Figure 8. Average particle axial velocity at 0.7 m (full line) and 2.2 m (dashed line) downstream of the diffuser (a). Contours of the average particle axial velocity inside the diffuser (b).

Attention is now driven to the velocity profiles within the diffuser body. In Fig. 9a, we show the mean gas profile at 5.08 m, that is, 0.08 m downstream of the diffuser inlet for both the single-phase and the particle–laden flow. The mass loading is kept at 0.5 and the roughness parameter is set at $\Delta\gamma = 1^o$ (smooth wall case) and $\Delta\gamma = 10^o$, referred to as rough wall case. Clearly, the fluid velocity becomes flatter as the wall roughness rises. The highly rough walls increase the gas axial velocity close to the walls and reduce it in the core flow. Figure 11b discloses a detached flow region in the single-phase simulation, which is slightly strengthened by the particles in the smooth case. This observation corroborates the explanation for the velocity profiles presented in Figs. 7 and 8: within the diffuser body, in certain regions which will be further explained with the aid of Fig. 15, the particles are faster than the gas, which is expanding. The drag force then becomes negative, that is, particles are decelerating and the gas is accelerating. Conversely, the momentum exchange term, given by Eq. (14), becomes positive in those zones. Since the gas flow rate is the same as in the single-phase flow, there will an increase in the gas velocity in this region and a reduction in the others. It is important to recall that the particles barely enter the recirculation region in the smooth wall case, as Fig. 8b shows. Interestingly, the reverse flow close to the wall is eliminated when the highly rough walls (10°) are used.

In order to explain the behavior above, the average particle axial velocity for the same section in both cases (smooth and rough walls) is shown in Fig. 10a. The particle velocity profile in the rough wall case is noticeably flatter than in the smooth wall case. Also, the particle velocity is much higher in the near-wall region, in which flow separation is known to occur in the single-phase simulation. This behavior is obviously owing to the high asperity of the walls, which enhance the particle collision frequency, with a resulting increase in the momentum exchange between particles. Consequently, a more uniform velocity distribution is expected, as reported by Laín *et al.* (2002) for horizontal channels. Small unphysical spikes, especially for the low roughness case, are visible in Fig. 10a. As will be seen in Fig. 10b, there are few particles in the near-wall zone, resulting in spurious statistics. Figure 10b displays the normalized particle concentration profiles for both smooth and rough walls. Unlike the smooth walls, the highly rough walls cause the particles to become more uniformly distributed across the diffuser body.

As previously mentioned, the high wall roughness increases the particle axial velocity in the near-wall region and decreases it in the core flow. The relative axial velocity will remain negative in this region, but its absolute value will be much higher when compared to the smooth wall case. Once again, regarding drag as the predominant force over the particles, it can be concluded that there will be a drag increase over particles in this region. The resulting effect will be an enhanced positive momentum transfer from the particles to the fluid in this region, see Eq. (14), up to the point that

a

b
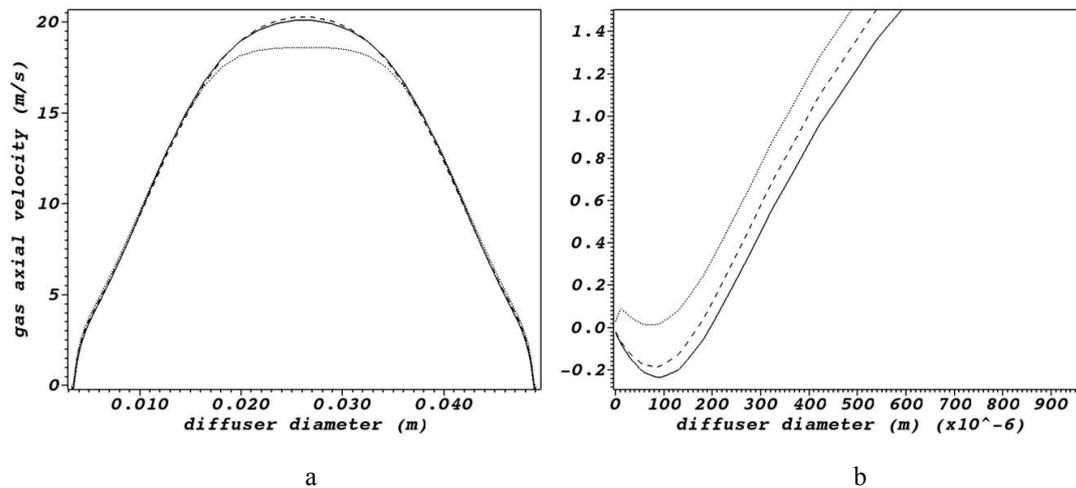
Figure 9. Average gas axial velocity inside the diffuser. Dashed line: unladen flow, full line: smooth wall ($\Delta\gamma = 1^o$), dotted line: rough wall ($\Delta\gamma = 10^o$).

a

b
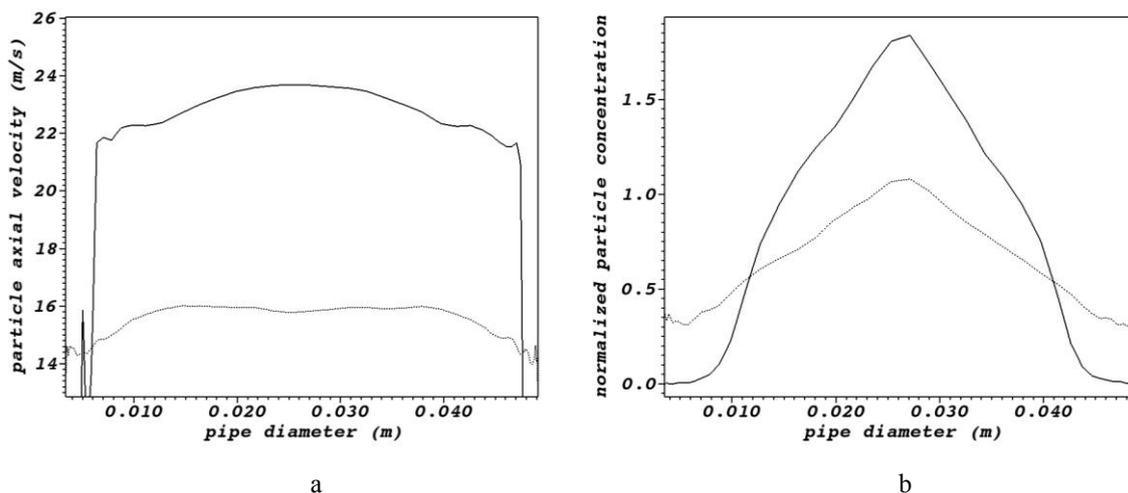
Figure 10. Average particle velocity (a) and normalized particle concentration (b) inside the diffuser. Full line: smooth wall ($\Delta\gamma = 1^o$), dashed line: rough wall ($\Delta\gamma = 10^o$).

the flow direction is inverted when compared to the single-phase flow. Naturally, the momentum exchange away from the walls, i.e., in the diffuser center, is reduced with respect to the low roughness case, which explains the more uniform gas velocity profile (Fig. 9).

This situation can also be interpreted in the light of the boundary layer theory. The flow separation in the diffuser is due to the adverse pressure gradient. The particles are in fact reinjecting momentum into the low-energy boundary layer, and this comes at the expense of an increased pressure gradient across the diffuser. Such increase of the pressure drop in channels with highly rough walls is reported by Laín *et al.* (2002). These authors explain that such rise is owing to the frequent inelastic collisions with the rough walls, which then decelerate the particles as they bounce back to the core flow. Therefore, more energy will be required for the particles to acquire the equilibrium velocity.

The importance of particle-to-particle collisions on the flow behavior is now investigated for the high roughness case. Figure 11 shows a comparison of the mean gas axial velocity considering and neglecting particle-to-particle collisions, that is, only a 2-way coupling. It can be noticed that the boundary layer still remains attached when interparticle collisions are not considered, although the velocity magnitude is lower in that region. This gives rise to a recirculation bubble between the wall region and the core flow. This result illustrates the relevance of including interparticle collisions in the modeling. For this mass loading, the volume fraction is only 0.00026. According to Elghobashi's diagram (1994), this would be considered a dilute suspension, and a two-way coupling should suffice. Nevertheless, such diagram is built assuming a homogeneous spatial distribution of the particles, which does not hold for the present case. The contours of the particle axial velocity for both two-way and four-way couplings are presented in Fig. 12. As expected from the previous discussions, in the absence of the interparticle collisions, the particle

Souza, F. J., Silva A, L. and Utzig, J.
Gas-particle flow in a diffuser

a

b
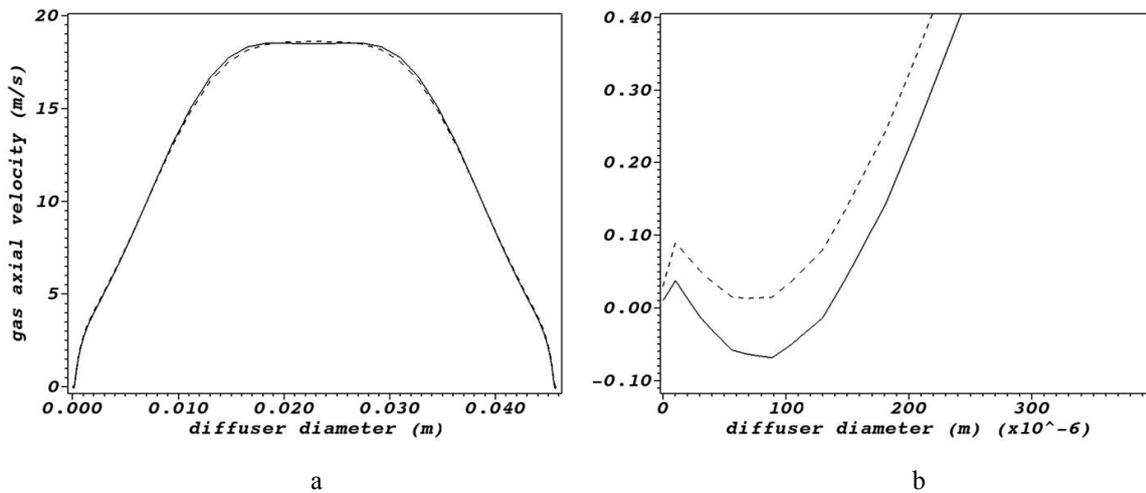
Figure 11. Average gas velocity inside the diffuser with rough walls for four-way (dashed line) and two-way (full line) simulations.

a

b
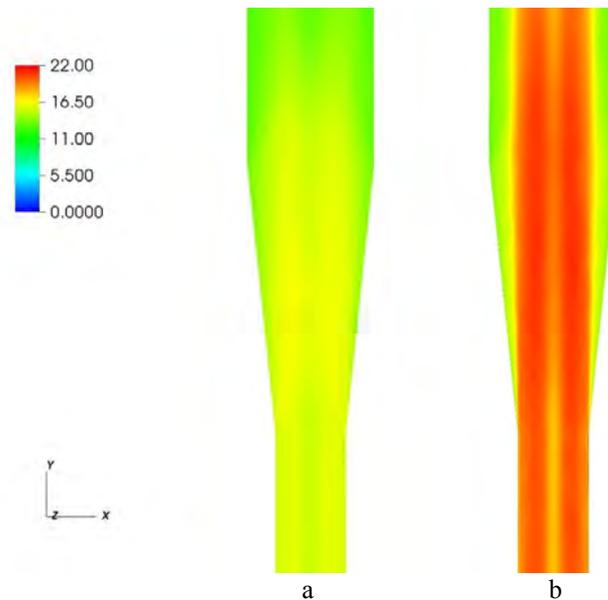
Figure 12. Contours of the axial particle velocity in the diffuser with rough walls for four-way (a) and two-way (b) simulations.

dispersion in the radial direction is severely decreased, and occurs mainly due to turbulence dispersion, which is not relevant for the rather inertial particles investigated in this work. Naturally, higher mass loadings will display a higher dependency on interparticle collisions.

Up to this point, it can be concluded that the key factor in the boundary layer reattachment within the particle-laden diffuser flow is the high surface roughness. However, it is important to bear in mind that this flow reattachment induced by particles and highly rough walls might not be possibly observed in a diffuser of larger diameter. When dealing with higher pipe diameters, the distance between colliding walls might be several orders greater than the particle mean path, meaning that mainly particles close to walls will be affected. Since interparticle collisions may play a secondary role in distributing the particles more homogeneously across the diffuser section, larger diffusers may not benefit from such effect.

For further clarification of the particle-induced reattachment mechanism, the horizontal flow in the same diffuser geometry is now simulated. Fig. 13 shows a comparison between the mean gas velocity for both the vertical and horizontal particle-laden flows with highly rough walls ($\Delta\gamma=10°$). It can be seen that also in the horizontal case the flow is reattached due to the particles and the high wall roughness, although the velocity magnitude in the proximity of the walls is lower compared to the vertical case. Nonetheless, this simulation corroborates the reattachment mechanism proposed.
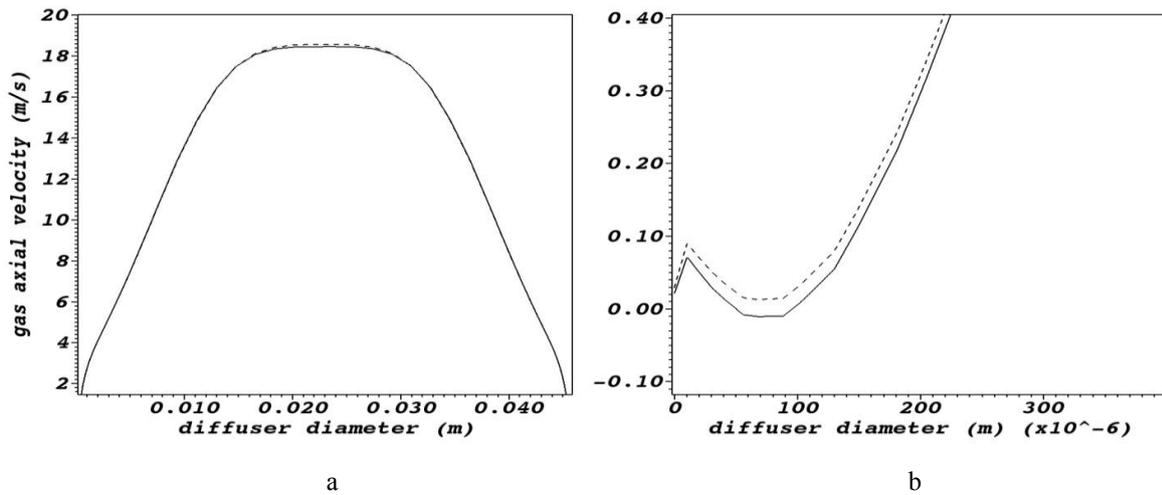
Figure 13. Average gas velocity inside the diffuser for horizontal and vertical flows with rough walls. Dashed line: vertical diffuser, full line: horizontal diffuser.

Finally, it is useful to investigate the relevance of the particle concentration in the flow. Figure 14 illustrates the effect of mass loading in the high roughness case. As expected from the mechanism proposed above, the gas velocity becomes more uniform, and the gas velocity is higher in the vicinity of the diffuser walls. Obviously, the favorable pressure gradient is higher. Therefore, it can be inferred that higher mass loadings can actually make both particle and gas velocity profiles almost flat, possibly eliminating the separation even in wider opening-angle diffusers. In fact, this was shown by the experiments carried out by Kale and Eaton (1985) downstream of a fluidized bed. Even the flow in a 60° opening angle diffuser was attached downstream of a fluidized bed. In that case, the surface roughness was probably not the factor uniformizing the particle distribution, since the diffuser width was 0.15 m and the effects of the wall irregularities would be restricted to the surface vicinity. Nevertheless, the fluidized bed itself induces very uniform properties due to thorough mixing, i.e., which implies very high frequency of particle collisions.

For further clarification, in Fig. 15 the contours of the particle average axial velocity for mass loadings 0.5 and 1.0 are displayed in the high roughness case. Besides the more homogeneous velocity distribution along a longer axial distance, it is also visible that the particle velocity actually increases with the mass loading. Because the particle velocity is generally higher in the near-wall zone, this is an interesting result especially for the boundary layer reattachment. Furthermore, this effect is not observed in a horizontal pipe or diffuser. An explanation based on the problem physics is the subject of an investigation by the authors.
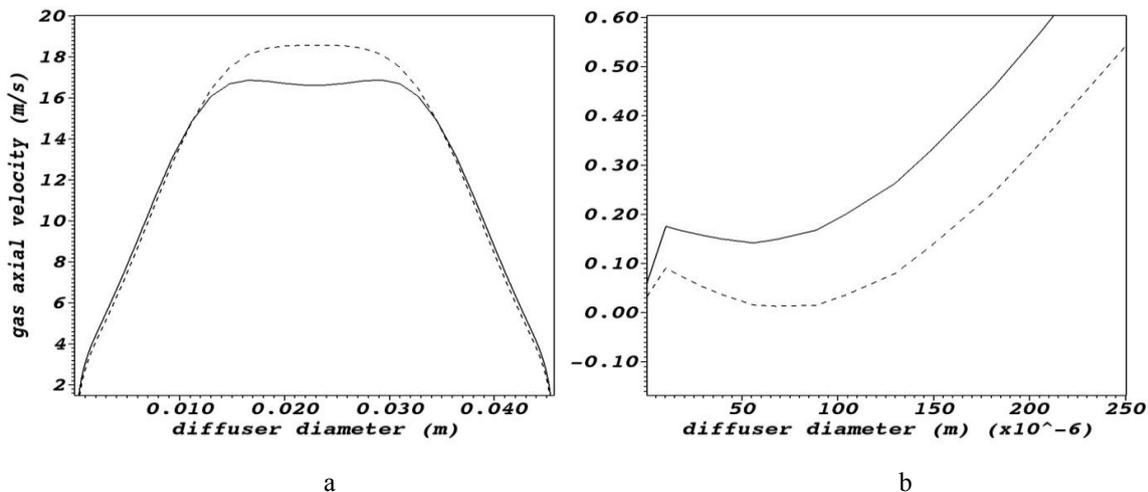
Figure 14. Average gas velocity inside the diffuser with rough walls ($\Delta\gamma =10^o$) due to different mass loadings: 0.5 – dashed line and 1.0 – full line.
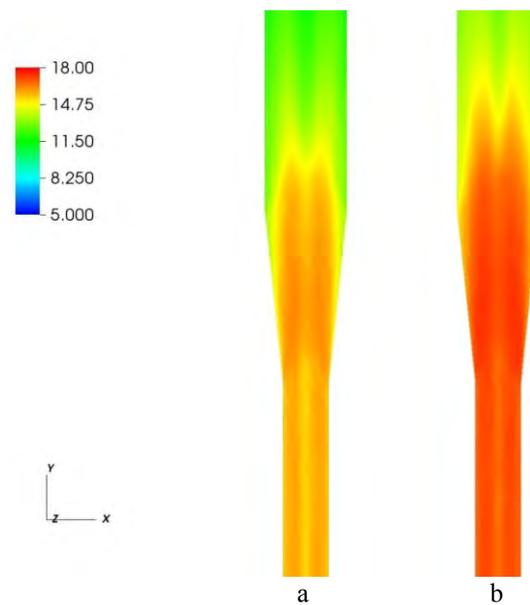
Figure 15. Contours of the particle phase axial velocity for mass loadings 0.5 (a) and 1.0 (b), rough wall case.

4. CONCLUSIONS

The simulation of both clean and particle-laden flow in a vertical diffuser was carried out. The code employs the Euler/Lagrange approach and was previously validated. Simulations show that the separated flow region in the vicinity to the diffuser wall is mitigated or eliminated, depending on the mass loading and the diffuser wall characteristics. An analysis of the results suggests that the main reason for the early flow reattachment is the homogenization of the particle concentration due to the wall roughness upstream of and across the diffuser section. Furthermore, it was found that mass loadings as low as 0.5 can significantly affect the flow behavior and eliminate the flow detachment depending on the diffuser wall characteristics. Essentially, the very frequent particle collisions promoted by the surface roughness provide momentum to the fluid boundary layer, overcoming the effect of the adverse pressure gradient across the diffuser. Interparticle collisions are shown to be quantitatively relevant even at moderate mass loadings.

5. REFERENCES

Bardina, J. E., Huang, P. G. and Coakley, T. J., 1997. "Turbulence Modeling Validation, Testing and Development". NASA TM 110446.

Benson, M., Tanaka, T., Eaton, J. K., 2005. "Effects of wall roughness on particle velocities in a turbulent channel flow". *Trans. ASME J. Fluids Eng.*, Vol. 127, p. 250-256.

Bohnet, M., Triesch, O., 2003. "Influence of Particles on Fluid Turbulence in Pipe and Diffuser Gas-Solids Flow". *Chem. Eng. Technol.*, Vol. 26, p. 1254-1261.

Breuer, M., Alletto, M., Langfeldt, 2012. "Sandgrain roughness model for rough wall within Eulerian-Lagrangian predictions of turbulent flows". *Int. J. Multiphase Flow*, Vol. 43, p. 157–175.

Breuer, M., Alletto, M. 2012. "Efficient simulation of particle-laden turbulent flows with high mass loadings using LES". *Int. J. Heat and Fluid Flow*, Vol. 35, p. 2–12.

Crowe, C.T., 2006. *Multiphase Flow Handbook*. CRC Press Taylor & Francis Group, Boca Raton, USA.

Crowe, C.T., Sommerfeld, M., Tsuji, Y., 1998. *Fundamentals of Gas-Particle and Gas-Droplet Flows*. CRC Press.

Dennis, S.C.R., Singh, S.N., Ingham, D.B., 1980. "The steady flow due to a rotating sphere at low and moderate Reynolds numbers". *J. Fluid Mech.*, Vol. 101, p. 257–279.

Elghobashi, S., 1994. "On predicting particle-laden turbulent flows". *Appl. Sci. Res.*, Vol. 52, p. 309-329.

Fessler, J. and Eaton, J. K., 1999. "Turbulence modification by particles in a backward-facing step flow". *J. Fluid Mech.*, Vo. 394, p. 97–117.

Ferziger, J. H., Peric, M., 2002. *Computational methods for fluid dynamics*. Springer, New York, 3th edition.

Haselbacher, A.,Najjar, F. M., Ferry, J. P., 2007. "An efficient and robust particle-localization algorithm for unstructured grids". *Journal of Computational Physics*, Vol. 225, p. 2198-2213.

Mathur, S. R., Murthy, J. Y., 1997. "A pressure-based method for unstructured meshes". *Numerical Heat Transfer, Part B,* Vol. 31, p. 195-215.

Kale, S. R. and Eaton, J. K., 1984. "An experimental investigation of gas-particle flows through diffusers in the freeboard region of fluidized beds". Report MD-45, Mechanical Eng. Dep., Stanford University, Stanford, CA.

22nd International Congress of Mechanical Engineering (COBEM 2013)
November 3-7, 2013, Ribeirão Preto, SP, Brazil

Kale, S. R. and Eaton, J. K., 1985. "An experimental investigation of gas-particle flows through diffusers in the freeboard region of fluidized beds". *Int. J. Multiphase Flow*, Vol. 11, p. 659-674.

Laín, S., Sommerfeld, M., 2013. "Characterisation of pneumatic conveying systems using the Euler/Lagrange approach". *Powder Technology*, Vol. 235, p. 764-782.

Laín, S., Sommerfeld, M., 2012. "Numerical calculation of pneumatic conveying in horizontal channels and pipes: Detailed analysis of conveying behavior . *Int. J. Multiphase Flow*, Vol. 39, p. 105–120.

Laín, S., Sommerfeld, M., Kussin, J., 2002. "Experimental studies and modelling of four-way coupling in particle-laden horizontal channel flow". *Int. J. Heat Fluid Flow*, Vol. 23, p. 647–656.

Lun, C. K. K. and Liu, H. S.,1997. "Numerical simulation of dilute turbulent gas-solid flows in horizontal channels". *Int. J. Multiphase Flow*, Vol. 23, p. 575-605.

Mei, R., 1992. "An approximate expression for the shear lift force on a spherical particle at finite Reynolds number". *Int. J. Multiphase Flow*, Vol. 18, p. 145–147.

Oesterlé, B., Petitjean, A., 1993. "Simulation of particle-to-particle interactions in gas-solid flows". *Int. J. Multiphase Flows*, Vol. 19, p. 199–211.

Rubinow, S.I., Keller, J.B., 1961. "The transverse force on a spinning sphere moving in a viscous liquid". *J. Fluid Mech.*, Vol. 11, p. 447–459.

Saffman, P.G., 1965. "The lift on a small sphere in a shear flow". *J. Fluid Mech.*, Vol. 22, p. 385–400.

Schiller, L., Naumann, A., 1935. "A drag coefficient correlation". *Z. Ver. Deutsch. Ing.*, p. 77-318.

Sommerfeld, M., 2001. "Validation of a stochastic Lagrangian modeling approach for inter-particle collisions in homogeneous isotropic turbulence". *Int. J. Multiphase Flow*, Vol. 27, p. 1829–1858.

Sommerfeld, M., Huber, N., 1999. "Experimental analysis and modelling of particle–wall collision". *Int. J. Multiphase Flow*, Vol. 25, p. 1457–1489.

Souza, F. J, Salvo, R. V and Martins, D. M. M., 2012. "Large Eddy Simulation of the gas-particle flow in cyclone separators". *Separation and Purification Technology*, Vol. 94, p. 61-70.

6. AKNOWLEDGEMENTS

7. RESPONSIBILITY NOTICE

The authors are the only responsible for the printed material included in this paper.